# THEORETICAL STUDIES OF OXYGEN DIFFUSION IN FACE-CENTERED CUBIC MATRICES OF XENON, ARGON, AND KRYPTON

By

M. BETH (BOLDING) FORD

Bachelor of Science

Oklahoma State University

Stillwater, Oklahoma

1982

Submitted to the Faculty of the
Graduate College of the
Oklahoma State University
in partial fulfillment of
the requirements for
the Degree of
MASTER OF SCIENCE
December, 1992

# THEORETICAL STUDIES OF OXYGEN DIFFUSION IN FACE-CENTERED CUBIC MATRICES OF XENON, ARGON, AND KRYPTON

Thesis Approved:

Lionel M. Raff
Thesis Advisor

Horacio A. Mottola

Donald L. Thompson

Thomas C. Collins
Dean of the Graduate College

ACKNOWLEDGEMENTS

I am grateful to Dr. Lionel M. Raff for the inspiration and supervision of this research project, and for the opportunity to complete the thesis requirements working in his area of research.

The loving support of my family in pursuing an education and career in chemistry is appreciated. My husband, Julian, was especially encouraging and helpful throughout my undergraduate and graduate studies.

The professional encouragement and financial support of Conoco Incorporated, with which I have been employed during the entire course of work toward the degree of Master of Science, is gratefully acknowledged, as well as the support and encouragement of my coworkers and supervisors at Conoco.

I am grateful for the availability of Oklahoma's Television Instruction System, and for the support of this system by Conoco, Inc. and Oklahoma State University, and for the efforts of instructors who work with the program.

I am thankful for the undergraduate and graduate advise and instruction I received between 1978 and 1992 at Oklahoma State University, especially from Dr. Raff, Dr. Horacio Mottola, and Dr. Tom Moore, and for the financial support of scholarships and a teaching and research assistantship during undergraduate studies.

TABLE OF CONTENTS

LIST OF TABLES

LIST OF FIGURES

# CHAPTER I

## INTRODUCTION

Information about the characteristics of atomic species such as oxygen atoms moving through a frozen rare-gas matrix is important in the quest for low-volume, high-energy fuel sources, and the search for high-energy density materials. It has been established that oxygen atoms can be "stored" in a solid matrix (1). Such a system can then be slowly warmed to allow the oxygen atoms to move and react at a controlled rate, releasing large amounts of energy at the desired time.

Krueger and Weitz (1) have provided an experimental basis for this work. In their experiments, oxygen atoms (as $N_2O$) were combined with xenon in a ratio of 1:729. Laser pulses were used to photolyze the $N_2O$ molecules producing oxygen atoms in the matrix. The diffusion and subsequent reaction of oxygen atoms to form molecular oxygen were observed to occur based on the measured time variation of the $O(^3P)$ concentration obtained from the photodetection experiments. The oxygen-atom decay was found to be nonlinear at both experimental temperatures, 32 K and 40 K. Two diffusion coefficients, representing an initial period of fast decay, followed by a period of slower decay, were

calculated to describe this nonlinearity. Krueger and Weitz (1) suggest two possible explanations for this multiple diffusion rate phenomenon (although only two diffusion rates were used to fit the data, they emphasize the possibility of multiple diffusion rates). First, the faster of the rates could be attributed to defects and inhomogeneities in the matrix which allow easier diffusion of some oxygen atoms. Second, the faster of the rates could result when oxygen atoms near each other combine, leaving the slower rate to represent atoms having to diffuse through more of the matrix before reacting.

The present theoretical study of the diffusion of an oxygen atom from one adsorption site to an adjacent adsorption site is designed to simulate diffusion in a perfect face-centered cubic (fcc) lattice. If diffusion rates slower than or similar to the slower rates reported by Krueger and Weitz (1) are obtained, the results will lend support to the first of the theories mentioned above, since our rates will represent diffusion in the absence of matrix defects. Conversely, theoretical diffusion matching the faster experimental rates will substantiate the second of the theories, since the reaction will have occurred between atoms in two adjacent adsorption sites.

Spath and Raff (2) have designed models involving multiple matrix zones, each individually homogeneous, but inconsistent with the other zones. These studies examine the kinetics of diffusion-controlled, bimolecular reactions

in inhomogeneous solid matrices with different types of defects. The findings have shown that diffusion-limited, radical recombination in an inhomogeneous matrix should not follow a simple, second-order rate law with a rate coefficient dependent upon a single diffusion coefficient. In the limiting case of various zones of matrix inhomogeneities, where interzone crossings are negligible, a distribution of diffusion coefficients may be extracted from an expansion of the data in terms of a power series on time.

In the present work, we employ classical variational transition-state theory to obtain estimates for diffusion rates of oxygen radicals in fcc matrices of rare gases at temperatures of 100, 150, and 200 K. Comparisons of results extrapolated from this data with the experimental data mentioned above are also given.

# CHAPTER II

## FORMULATION OF MODEL

### Matrix Model

The rare-gas matrix was simulated by a (5X5) fcc lattice. The unit cell spacings were adopted from Raff (3), who has shown that the limited 5X5 lattice size introduces only negligible errors. The unit cell spacings used to set up the fcc matrix are listed in Table I with the initial Leonard-Jones potential energies of the xenon, argon, and krypton matrices in this configuration.

TABLE I

UNIT CELL SPACINGS FOR FCC MATRIX CONFIGURATION AND POTENTIAL ENERGY SUMS OF (5X5) MATRICES

| Matrix | Unit Cell Spacing (Angstroms) | Potential Energy of 5X5 fcc (eV rel. to infinite separation) |
|---|---|---|
| Xenon | 6.132 | -89.4 |
| Argon | 5.438 | -37.6 |
| Krypton | 5.646 | -64.2 |

The energies were calculated by summing the van der Waals forces between each pair of atoms using the Leonard-Jones potential energy equation,

$$V(i,j) = D[(\frac{R_e}{R})^{12} - 2(\frac{R_e}{R})^6], \quad (1)$$

for $R \leq R_{cut}$. V(i,j) represents the pairwise potential energy between atoms i and j; D is defined as the energy difference between infinite and equilibrium separation of two atoms; $R_e$ is the equilibrium distance predicted by the pairwise potential between the two atoms; and R is the actual distance between the two atoms (4). For each matrix, a maximum separation, $R_{cut}$, was used as a cutoff to reduce the computational requirements; the potential between pairs of greater separation were considered negligible; V(i,j) = 0 for $R(i,j) \geq R_{cut}$ (3).

The values of the parameters used for these evaluations are given in Table II.

The entries in Table II labelled "(C)" are values computed using standard combining rules. For the distance parameter, we employ

$$(R_e)_{AB} = [(R_e)_{AA} + (R_e)_{BB}]/2. \quad (2)$$

For the energy parameter, the combining form used is

$$D_{AB} = [(D_{AA}) \times (D_{BB})]^{\frac{1}{2}}. \quad (3)$$

TABLE II

PARAMETERS USED FOR MATRIX-MATRIX AND MATRIX-OXYGEN INTERACTIONS

| Interaction | Re (Angstroms) | D (eV) | $R_{cut}$ (Angstroms) |
|---|---|---|---|
| Xenon-Xenon | 4.362 (3) | 0.024214 (3) | 7.0(3) |
| Xenon-Oxygen | 3.727 (C) | 0.0075702 (C) | |
| Argon-Argon | 3.810 (3) | 0.010288 (3) | 6.0(3) |
| Argon-Oxygen | 3.451 (4) | 0.0053768 (4) | |
| Krypton-Krypton | 4.007 (3) | 0.01738 (3) | 6.4(3) |
| Krypton-Oxygen | 3.549 (C) | 0.0064133 (C) | |

Figures 1-3 of the appendix show plots of potential energy vs. atomic separation [V(i,j) vs. R(i,j)] for each matrix element.

During the diffusion of the oxygen atom, the lattice atoms are allowed to move subject to a canonical probability distribution. Moves which adversely effect the stability of the system are usually not accepted, and the movement of atoms beyond the initial outer boundary of the matrix is prohibited. Since the fcc configuration is most stable, the atoms remain roughly in this configuration with the exception of some movement or "relaxation" around the oxygen atom.

## Oxygen Atom

The oxygen atom is inserted at the center-most adsorption (low-potential) site, or the mid-point of the center unit cell. The objective of the study is to compute the diffusion rate to an adjacent adsorption site, which, in a fixed matrix, would be located at the mid-point of an edge of the center cell as illustrated in Figure 4 of the appendix. Because of the symmetry of the fcc matrix, this point is theoretically equivalent to the initial location of the oxygen atom before relaxation of the lattice atoms, although the finite size of the model introduces a small deviation from the expected symmetry. Oxygen-matrix interaction parameters are included in Table II, and Figures 5-7 of the appendix illustrate the diatomic oxygen-xenon, oxygen-argon, and oxygen-krypton potential energy interactions [V(i,oxygen) vs. R(i,oxygen)], respectively.

## Variational Phase-Space Theory Calculations

The diffusion rate of the oxygen atom is calculated from the jump frequency, or flux, across a theoretical dividing surface separating two adsorption sites. The principle of variational transition-state theory is that this flux must be an upper limit to the actual rate since all reactions involve crossing the dividing surface but not all crossings of the surface result in reaction. Consequently, we seek the dividing surface that minimizes the flux. Several spherical and cubical surfaces are tested to

determine the surface that yields the lowest flux. After this determination is made, the flux across the optimum dividing surface is considered to be the jump frequency most closely approximating experiment. The effects of temperature on the flux are also examined.

The total energy of the system is given by Eqs. (4) and (5), where N represents the total number of lattice atoms {666 in a (5X5) fcc matrix}; $P_{qi}$ = the momentum of atom i in the q direction; x, y, and z = Cartesian coordinates; i and j represent matrix atoms and r represents the oxygen atom; m = mass; and V = potential energy.

$$E=T(kinetic\ energy)+V(potential\ energy) \tag{4}$$

$$E=\sum_{i=1}^{N}\left(P_x^2+P_{yi}^2+P_{zi}^2\right)/2m_i+\left(P_{xr}^2+P_{yr}^2+P_{zr}^2\right)/2m_r+\frac{1}{2}\sum_{i=1}^{N}\sum_{j=1}^{N}V_{ij}+\sum_{i=1}^{N}V_{ir} \tag{5}$$

The energy involved in the movement of the oxygen and lattice atoms is thermal. Therefore, a Boltzmann distribution of energies (canonical) is assumed. The jump frequency (probability of moving from one adsorption site to another) is proportional to the probability of the atom being in the critical area and to the velocity of the atom perpendicular to the dividing surface. The jump frequency can be written mathematically as the ratio of the summation over positions involving jumps (and possible reaction) to the summation over the total available phase-space volume. If F(T) is the flux at temperature T, we have Eq. (6), where the delta

function is unity when on the dividing surface.

$$F(T) = \frac{\int_p \int_q e^{-E/kT} |V_\perp| \, \delta(q-q_0) \prod_{i=1}^{3N} dq_i dp_i}{\int_p \int_q e^{-E/kT} \prod_{i=1}^{3N} dq_i dp_i} \tag{6}$$

The integrations over momenta in Eq. (6) can all be done analytically. This integration over momenta yields the average velocity, and Eq. (6) assumes the form

$$F(T) = \langle v \rangle \frac{\int_q e^{-E/kT} \delta(q-q_0) \prod_{i=1}^{3N} dq_i}{\int_q e^{-E/kT} \prod_{i=1}^{3N} dq_i}, \tag{7}$$

where <v> represents the average velocity of the oxygen atom, given by

$$\langle v \rangle = \left[\frac{8kT}{\pi m_r}\right]^{\frac{1}{2}}. \tag{8}$$

Since the potential being employed is separable into a lattice potential plus an oxygen atom-lattice interaction term (6), we may write

$$V = V_L + V_O , \tag{9}$$

where

$$V_L = \frac{1}{2} \sum_{i=1}^{N} \sum_{j=1}^{N} V_{ij} , \tag{10}$$

and

$$V_O = \sum_{i=1}^{N} V_{ir} . \tag{11}$$

Substitution of Eqs. (9)-(11) into Eq. (7) yields

$$F(T) = \langle V \rangle \frac{\int_q e^{-V_I/kT} e^{-V_o/kT} \delta(q-q_0) \prod_{i=1}^{3N} dq_i}{\int_q e^{-V_I/kT} e^{-V_o/kT} \prod_{i=1}^{3N} dq_i}. \qquad (12)$$

The complexity of the potential precludes analytical evaluation of Eq. (12). We therefore utilize Monte Carlo sampling methods to execute the required integration (5). To do this, we first replace the dividing surface with a dividing "slab" of width $\Delta w$. If $\Delta w$ is sufficiently small that the integrand of Eq. (12) is constant across the width, Eq. (12) becomes

$$F(T) = \frac{\langle V \rangle}{\Delta w} \frac{\int_q e^{-V_I/kT} e^{-V_o/kT} \delta(\Delta w) \prod_{i=1}^{3N} dq_i}{\int_q e^{-V_I/kT} e^{-V_o/kT} \prod_{i=1}^{3N} dq_i}, \qquad (13)$$

where $\delta(\Delta w)$ is unity if a configuration point lies within the dividing slab. Otherwise, $\delta(\Delta w)$ is zero.

Equation (13) may be evaluated by a random sampling of points within the unit cell and dividing volume. The Monte Carlo approximant for the integrals gives Eq. (14), where M is the total number of Monte Carlo points sampled.

$$F(T) = \frac{\langle V \rangle}{\Delta w} \frac{\frac{1}{M} \sum_{i=1}^{M} e^{-V_I/kT} e^{-V_o/kT} \delta(\Delta w)_i}{\frac{1}{M} \sum_{i=1}^{M} e^{-V_I/kT} e^{-V_o/kT}} \qquad (14)$$

In this form, the convergence of the summation will be

much too slow if the Monte Carlo walk is allowed to progress entirely at random. The convergence rate may be significantly increased by sampling the lattice configuration from a canonical probability density distribution. That is, we select the configuration using a probability function of the form

$$P(q) = ce^{-V_L/kT}, \tag{15}$$

where c is a normalization constant.

In practice, the configuration points are obtained using a canonical Markov walk in which n (typically 10-20) lattice atoms are randomly selected and then moved according to

$$q_i^{new} = q_i^{old} + \xi_i \Delta Q(probability\ function), \tag{16}$$

where i = 1,2,3...n and $\xi_i$ is a random number selected from a uniform distribution on the interval [0,1], $q_i^{old}$ is the old x, y, or z-coordinate of atom i, and $q_i^{new}$ is the new coordinate. The probability function is discussed below. After the lattice atoms are moved, the new potential energy of the lattice is calculated. If the probability of the lattice having this energy is greater than the probability of the lattice having the energy of the previous arrangement, the move is accepted; i.e., accept if

$$e^{-V_L(new)/kT} \geq e^{-V_L(old)/kT}. \tag{17}$$

A canonical distribution of the configuration points will be

generated in the walk if the move is also accepted whenever

$$\frac{e^{-V_L(new)/kT}}{e^{-V_L(old)/kT}} \geq \xi . \tag{18}$$

All other moves are rejected and a new move is attempted.

If configuration space is sampled via the above Markov walk, Eq. (14) becomes

$$F(T) = \frac{1}{2}\frac{\langle v \rangle}{\Delta w}\frac{\frac{1}{M}\sum_{i=1}^{M}\left[e^{-V_o/kT}\delta(\Delta w)\right]_i}{\frac{1}{M}\sum_{i=1}^{M}\left[e^{-V_o/kT}\right]_i} . \tag{19}$$

The factor of ½ is included to correct for entries into the dividing volume in the wrong direction. The jump frequencies computed in this study were obtained using Eq. (19).

In the execution of the Markov walk, the step size of the atoms as they move, $\Delta Q$, is chosen to optimize samplings of the system. The number of lattice atoms moved with each iteration of the process and the maximum step size of those moves are adjusted to keep the number of accepted and rejected moves approximately equal. Ten lattice atoms are typically moved and tested for probability. If the energy change is acceptable, the oxygen atom is moved and the new location evaluated for any contribution to the diffusion rate. Most of the tests are performed with a maximum step size equal to 2% of the unit cell spacing, though the oxygen atom is moved up to 8% of the unit cell spacing for xenon to improve convergence.

The angles at which the atoms are moved are chosen using Eqs. (20) and (21). The new coordinates are defined by Eqs. (22) - (24).

$$\phi = 2\pi\xi \tag{20}$$

$$\theta = \cos^{-1}[1-2\xi] \tag{21}$$

$$\Delta x = \Delta Q \sin\theta \cos\phi \tag{22}$$

$$\Delta y = \Delta Q \sin\theta \sin\phi \tag{23}$$

$$\Delta z = \Delta Q \cos\theta \tag{24}$$

Equation (21) selects the azimuthal angle from a distribution weighted by sin $\theta$. Since the volume element is proportional to sin $\theta$, Eqs. (20) and (21) are selecting the angles from the appropriate distribution.

The surfaces for which the flux is determined are actually volumes, the width ($\Delta w$) of which is determined by the maximum step size of the oxygen atom. The width of the dividing surface is designed to be no smaller than this step size to ensure that the oxygen atom cannot move from one side of the dividing volume to the other without entering the volume. The rate of convergence of Eq. (19) is determined by the number of moves required to sample the lowest-energy areas of the dividing volume described earlier.

The symmetry of the fcc matrix leads to the expectation that the interaction of the oxygen atom with the matrix (assuming a fixed matrix) as it travels along a line toward an adjacent (and identical) adsorption site, will be the mirror image of itself at the midpoint. Deviations from this can result from relaxation of the lattice atoms. The oxygen atom move is rejected if it calls for coordinates beyond the outer boundary of the outer-most dividing surface being tested.

Most of the tests were conducted with concentric spherical boundaries. Cubical dividing volumes were included in initial tests, but resulted in higher fluxes. Five spheres, with diameters equal to 0.1, 0.3, 0.5, 0.7, and 0.9 times the unit cell spacing, respectively, were tested most extensively. The dividing volumes are represented graphically in Figure 8 of the appendix.

## Diffusion Rate

Because the ratio of oxygen atoms to the number of adsorption sites is small, the diffusion coefficient can be related to the jump frequency, F, by the equation

$$D = \frac{d^2 F \theta}{\alpha}, \qquad (25)$$

where d is the diffusion length (distance between adjacent adsorption sites), $\Theta$ is the fraction of vacant sites (=1), and $\alpha$ is the dimensionality factor, which is three since the oxygen atom is allowed to move in any direction (6). Fac-

tors of $(10^{-8})^2$ and $(1.019 \times 10^{-14})^{-1}$ must be included to convert $(\text{angstroms})^2$ to $cm^2$ and time units to seconds, respectively.

The contribution of tunnelling to the diffusion was not considered because of the mass of the oxygen atom.

# CHAPTER III

## RESULTS AND DISCUSSION

### Convergence of the Flux Integrals

The rate of convergence of the flux integrals is dependent upon the number of iterations of the oxygen-atom movement and potential-energy summation required before the areas of minimum potential energy are found for the dividing volume being tested. The minimum potential energies observed for each of the dividing volumes in each matrix at 100 K are shown in Table III.

TABLE III

POTENTIAL AND DIFFUSION DATA FOR FIVE SURFACES AT 100 K

| Dividing Surface: | | A | B | C | D | E |
|---|---|---|---|---|---|---|
| Matrix(#Accepted Moves) | | | | | | |
| Xenon (.51M) | Min. Potential,eV | .23 | .42 | .66 | .73 | .59 |
| | Flux,jumps/time | 6E-06 | 2E-15 | 1E-27 | 4E-31 | 1E-22 |
| | Diffusion,$cm^2/s$ | 3E-07 | 9E-17 | 6E-29 | 2E-32 | 7E-24 |
| Argon (.83M) | Min. Potential, eV | .36 | .72 | 1.13 | 1.28 | .86 |
| | Flux,jumps/time | 4E-06 | 2E-24 | 3E-45 | 2E-52 | 2E-31 |
| | Diffusion,$cm^2/s$ | 2E-07 | 9E-26 | 1E-46 | 8E-54 | 1E-33 |
| Krypton (.46M) | Min. Potential,eV | .41 | .79 | 1.41 | .95 | .79 |
| | Flux,jumps/time | 8E-10 | 6E-29 | 2E-60 | 4E-37 | 3E-29 |
| | Diffusion,$cm^2/s$ | 4E-11 | 3E-30 | 1E-61 | 2E-38 | 2E-30 |

The 100 K xenon data are also shown graphically as a function of accepted moves, M, in Figure 9 of the appendix. Initial computations at temperatures near those used experimentally were unsuccessful because of extremely slow convergence. Convergence also appears less complete for the outermost dividing volumes with the 0.5 to 1.5 million moves used in the tests. This might be expected because of the larger areas to be sampled in the outer dividing volumes. Figure 10 of the appendix shows the minimum potential energies sampled for each of the dividing surfaces for xenon at the three temperatures. The fact that surface "D" shows the highest barrier at 100 K is attributed to a lack of convergence caused by the fewer moves sampled, the larger area of the boundary relative to boundaries "A" through "C", and the lower temperature. Convergence was also hindered in the initial experiments by not limiting matrix atoms to movement within the initial lattice boundary. The system potential dropped steadily as the lattice slowly disintegrated, and convergence was not achieved.

Because of the exponential dependence of the flux on the system energy, computational difficulties (numerical overflows) were encountered as the minimum energy decreased throughout the run. Compensating factors were included in the program calculations to counter the overflow. There were some cases in which the overflow continued to be a problem, and in these instances, the minimum potential sampled was used in the flux equation. The data in Figure

11 of the appendix demonstrates that only an infrequent and small (relative to the results of the experiment) change is observed in the numerator sum while the minimum potential remains constant.

## Potential Barriers to Diffusion

The potential energy of the system as the oxygen atom moves within the center unit cell varies considerably from the adsorption sites to locations near a matrix atom. If the oxygen were to move along a straight line in the x-y plane from one adsorption site to another in a fixed xenon lattice, the potential energy of the system would vary in the manner shown by Figure 12 of the appendix. The potential energy along this path is maximum when the oxygen atom is centered between the two closest face atoms. This potential variation in a fixed lattice leads to the expectation that the barrier of minimum flux would be closely approximated by that sphere centered between two adsorption sites.

The diffusion rates calculated for each of the dividing widths described earlier are included in Table III. Surface "C", a sphere of diameter 0.50x(unit cell length), had the highest barrier to diffusion in only one of the cases cited. These results deviate from those expected on the basis of symmetry considerations. The differences are assumed to be the result of slower convergence for the outer volumes (as discussed earlier--refer again to Figure 10) and/or matrix relaxation. Because of the possibility of non-convergence

in surface "D", the xenon data treatment was performed using surface "C".

The spaciousness of the three matrices (proportional to the unit cell sizes) would lead to the expectation that diffusion would occur most easily in the xenon matrix, followed by the krypton and argon matrices, respectively. The deviations observed from this expectation are also a result of lack of convergence and/or the effects of the relatively high lattice temperatures. These temperature effects are discussed below.

## Effects of Temperature on Diffusion

Calculations were performed at 100, 150, and 200 K. The results of the variational transition-state calculations for Surface "C" are tabulated in Table IV for xenon and krypton and plotted for xenon in Arrhenius form in Figure 13 of the appendix.

TABLE IV

DIFFUSION RATES, $cm^2/s$ VS. TEMPERATURE, K
SURFACE "C"

"( )" represents the number of moves used in each case.

| | 100K | 150K | 200K |
|---|---|---|---|
| XENON | $6.6 \times 10^{-29}$(.5M) | $3.0 \times 10^{-22}$(.9M) | $1.4 \times 10^{-13}$(1M) |
| KRYPTON | $1.3 \times 10^{-61}$(.5M) | not computed | $1.0 \times 10^{-34}$(.6M) |

Because the computations were performed near or above the boiling points of the matrices (m.p. xenon = 161 K, argon = 84 K, krypton = 116 K) to achieve convergence, some of the data reflect a mix between solid-state and gaseous diffusion rates. As such, these data are not representative of solid-state matrix diffusion. This is the case for all of the argon data and most of the krypton data. However, both the 100 and 150 K data points for xenon lie below the boiling point. Consequently, this data is used most extensively in the analysis. An attempt was made to obtain the diffusion rate in Xe at 80 K, but convergence was too slow.

As can be seen from Table IV, the diffusion rates are very low for both krypton and xenon matrices, although they are significantly higher for the more spacious xenon lattice, as expected (argon data is not included for reasons discussed above). A least-squares fit to the xenon data shown in Figure 11 yields a diffusion coefficient in xenon of

$$D_{Xe}(T) = 1.29 \exp[-13.29 \text{ kcal/mol/RT}] \text{ cm}^2/\text{sec}.$$

The result at T = 200 K for xenon is suspect since this temperature lies above the melting point of the matrix. An inspection of Figure 11 shows that the calculated rate at 200 K is greater than the data at 100 and 150 K suggest it should be. If the result at 200 K is discarded, the temperature dependence of $D_{Xe}(T)$ becomes

$$D_{Xe}(T) = 6.1 \times 10^{-9} \exp[-9.15 \text{ kcal/mol/RT}] \text{ cm}^2/\text{sec}.$$

## Comparisons to Experimental Data

Krueger and Weitz (1) have extracted diffusion coefficients for oxygen atoms in xenon matrices at 32 and 40 K from the results of their recombination rate measurements. Their data indicate that a distribution of such diffusion coefficients exists. By assuming that the distribution can be adequately represented by two coefficients, they obtain the values given in Table V. The extrapolated values at 32 and 40 K obtained from the least-squares fit to the variational transition-state results for xenon with and without including the result computed at a lattice temperature of 200 K are also given in Table V for comparison.

TABLE V

COMPARISON OF EXPERIMENTALLY AND THEORETICALLY DETERMINED DIFFUSION RATES FOR OXYGEN DIFFUSION IN XENON

| Temp, K | Diffusion Rate, D, $cm^2/s$ | | | |
|---|---|---|---|---|
| | Experimental (1) | | Variational Transition-State | |
| | Fast | Slow | with 200 K data | without 200 K |
| 32 | $1.4 \times 10^{-15}$ | $5.4 \times 10^{-18}$ | $2.5 \times 10^{-91}$ | $2.4 \times 10^{-71}$ |
| 40 | $7.3 \times 10^{-15}$ | $2.0 \times 10^{-17}$ | $3.5 \times 10^{-73}$ | $7.2 \times 10^{-59}$ |

Although the statistical error in the variational transition-state results leads to a large uncertainty in the extrapolated rates at 32 and 40 K, it is nevertheless clear that neither of the diffusion rates obtained from the exper-

imental $O_2$ recombination rate measurements (1) corresponds to diffusion in an fcc xenon lattice. At 32 K, the experimental rates are between 56 to 77 orders of magnitude faster than those for a perfect fcc lattice depending upon which extrapolated value is used. At 40 K, the differences are between 42 and 56 orders of magnitude.

Obviously, **all** of the diffusion occurring in the experimental matrices is taking place along defect pathways related to the imperfections in the structure of the vapor-deposited matrices. Recent theoretical studies by Raff (7) have shown that such defects are expected to be extensive with approximately three vacancies about each xenon lattice atom. The present results show that the experimental matrices must contain numerous imperfections, possibly even more extensive than indicated by the Monte Carlo simulations (7).

A comparison of the calculated and experimental activation energies leads to the same conclusion. The transition-state calculations lead to an activation barrier in xenon that lies in the range $9.1 \leq E_a \leq 13.3$ kcal/mol, depending upon whether one discards the rate computed at a lattice temperature of 200 K or not. In contrast, the temperature dependence observed by Krueger and Weitz (1) yields $0.41 \leq E_a \leq 0.53$ kcal/mol. Such a low activation energy shows that diffusion must be occurring exclusively along the defect pathways present in the lattice. Our results show that in a bulk fcc crystal, the activation barrier must be at least an order of magnitude larger.

# CHAPTER IV

## SUMMARY

The thermal diffusion of oxygen atoms in cryogenic matrices of argon, krypton, and xenon has been investigated using classical variational transition-state theory methods. The rare-gas matrices are represented by a 666-atom ensemble in an fcc configuration. A total of 125 unit cells in a (5x5x5) configuration are modeled. The oxygen atom is placed at the center of the innermost unit cell which represents the most stable adsorption site. The lattice is allowed to relax as the oxygen atom is moved randomly within the cell. A Markov walk is employed to evaluate the multidimensional configuration space integrals required for computation of the variational flux. The highest barrier to diffusion is determined by calculating the system potential energy as the oxygen atom crosses a series of dividing surfaces separating its initial location from an adjacent adsorption site. The diffusion rate of the oxygen atom is determined from the flux across the highest potential dividing surface between adsorption sites.

The results yield a diffusion coefficient in xenon

$$D_{Xe}(T) = 1.29 \exp[-13.29 \text{ kcal/mol/RT}] \text{ cm}^2/\text{sec}.$$

Diffusion rates in krypton are even slower. If the diffusion rate in xenon computed at a lattice temperature of 200 K is omitted from the data set because such a lattice temperature lies above the experimental melting point of a xenon matrix, the calculated diffusion rate becomes

$$D_{Xe}(T) = 6.1 \times 10^{-9} \exp[-9.15 \text{ kcal/mol/RT}] \text{ cm}^2/\text{sec}.$$

Thus, we find the activation energy for oxygen-atom diffusion in an fcc xenon matrix to lie in the range $9.1 \leq E_a \leq 13.4$ kcal/mol.

A comparison of the variational transition-state theory results with values determined experimentally by Krueger and Weitz (1) shows that the experiments are not monitoring bulk diffusion in fcc matrices. The experimental rates are many orders of magnitude faster than those obtained for fcc matrices. The much slower diffusion rate in fcc matrices is the result of the perfection (or lack of defects) of the matrix environment. In contrast, the experimental matrix contains grain boundaries, missing atoms, and other imperfections which result in higher diffusion rates (7). These larger rates are reflected in the activation energies reported by Krueger and Weitz (1) which are more than an order of magnitude less than those obtained for the fcc matrix.

It is concluded that **all** of the diffusion taking place in the experimental matrices (1) is occurring along pathways related to the lattice defects. Therefore, it is incorrect to conclude that the "fast" rate coefficient reported by Krueger and Weitz (1) for oxygen-atom diffusion in xenon

represents diffusion along defects and inhomogeneities in the matrix, while the "slow" coefficient corresponds to diffusion in a bulk fcc matrix environment. It appears that the experimental situation corresponds to one in which there is a distribution of rate coefficients present that is characteristic of the distribution of defects types and number in the lattice (2). The "slow" and "fast" values extracted by Krueger and Weitz (1) are best viewed as representing average values of this distribution over the low and high ends of the distribution, respectively.

## REFERENCES


1. H. Krueger and E. Weitz, J. Chem. Phys., **92**, 2846 (1992).

2. B. W. Spath and L. M. Raff, J. Phys. Chem., **96**, 2179 (1992).

3. L. M. Raff, J. Chem. Phys., **93**, 3160 (1990).

4. R. Gunde, P. Felder, and Hs. H. Günthard, Chemical Physics, **64**, 313 (1982).

5. L. M. Raff and D. L. Thompson, "The Classical Trajectory Approach to Reactive Scattering", in **Theory of Chemical Reaction Dynamics**, M. Baer (Ed.), Vol. III, (CRC Press Inc., Boca Raton, Fl.), p. 1.

6. I. NoorBatcha, L. M. Raff, and D. L. Thompson, J. Chem. Phys., **81**, 3715 (1984).

7. L. M. Raff, J. Chem. Phys., **98**, 0000 (1993).

# APPENDIX

## FIGURES

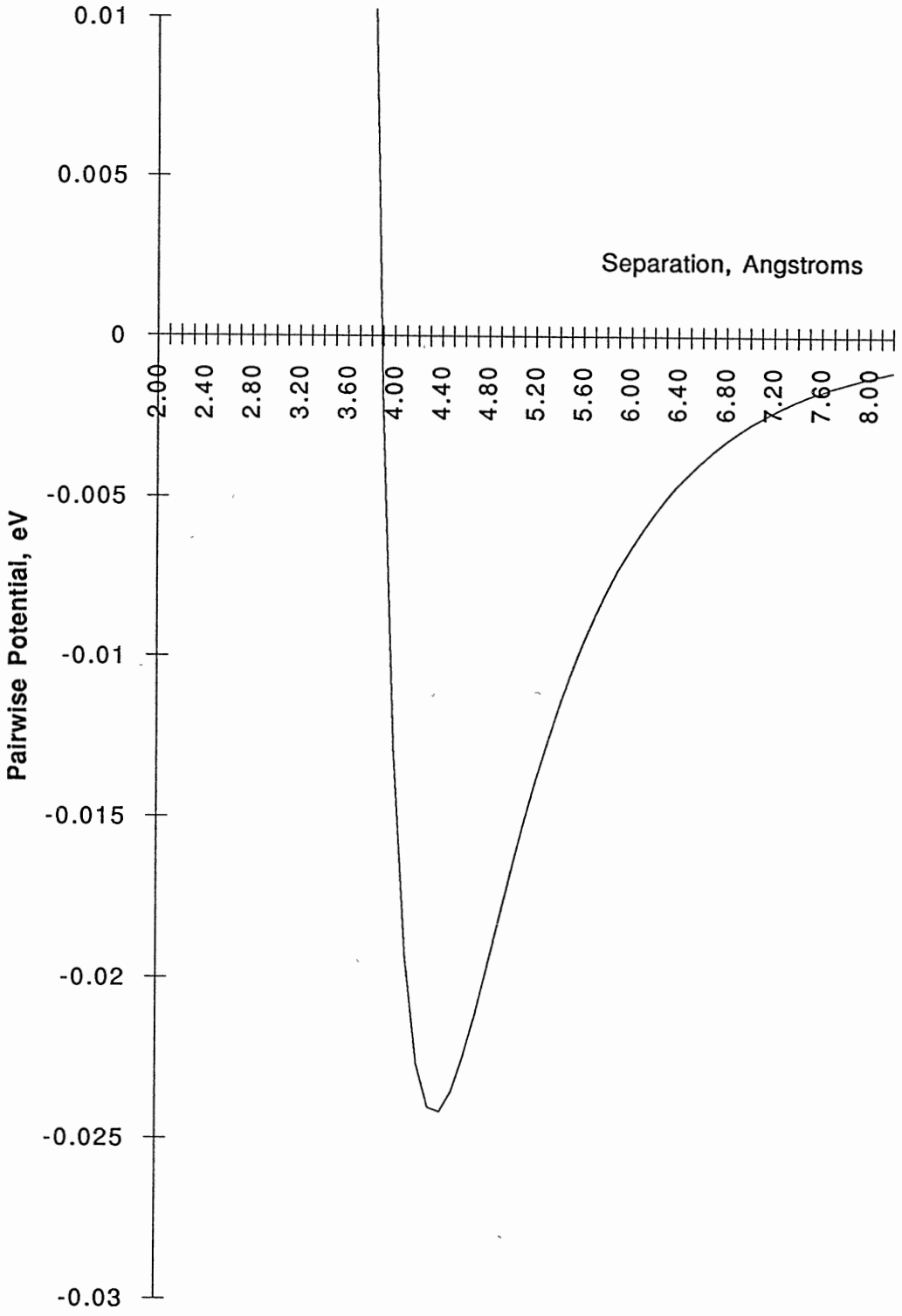


Figure 1. Potential Energy vs. Diatomic Separation for Xenon-Xenon

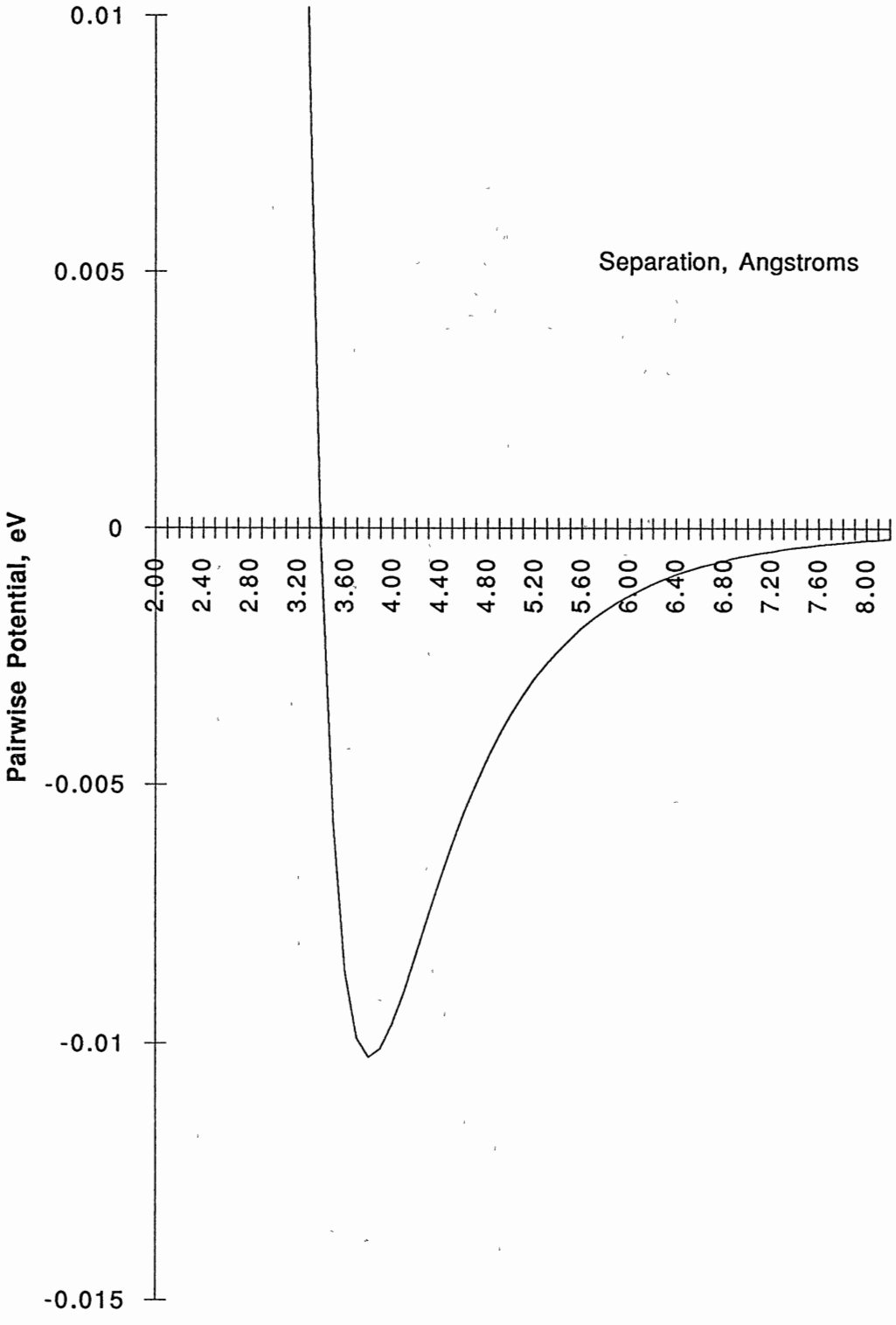


Figure 2. Potential Energy vs. Diatomic Separation for Argon-Argon

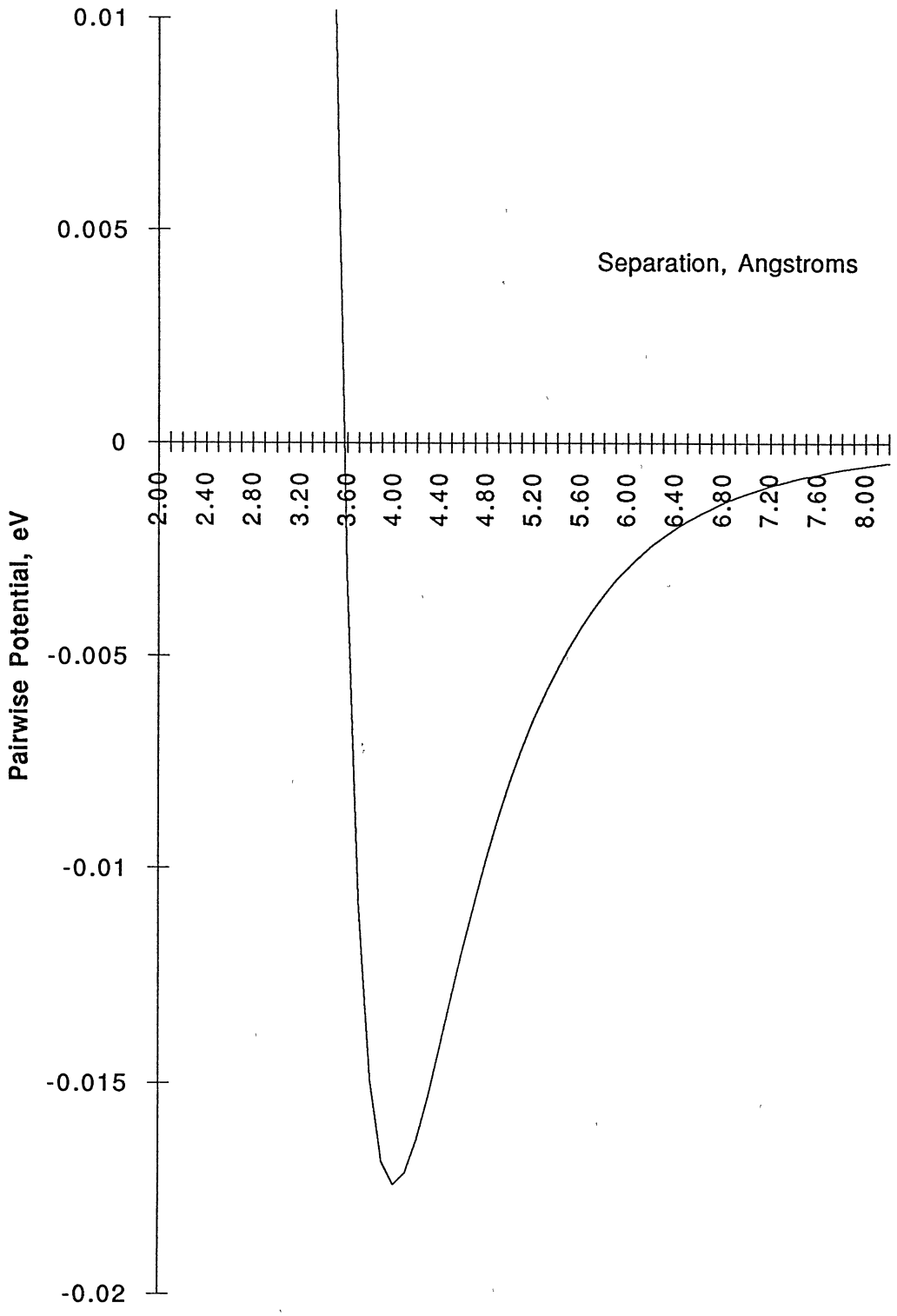


Figure 3. Potential Energy vs. Diatomic Separation for Krypton-Krypton

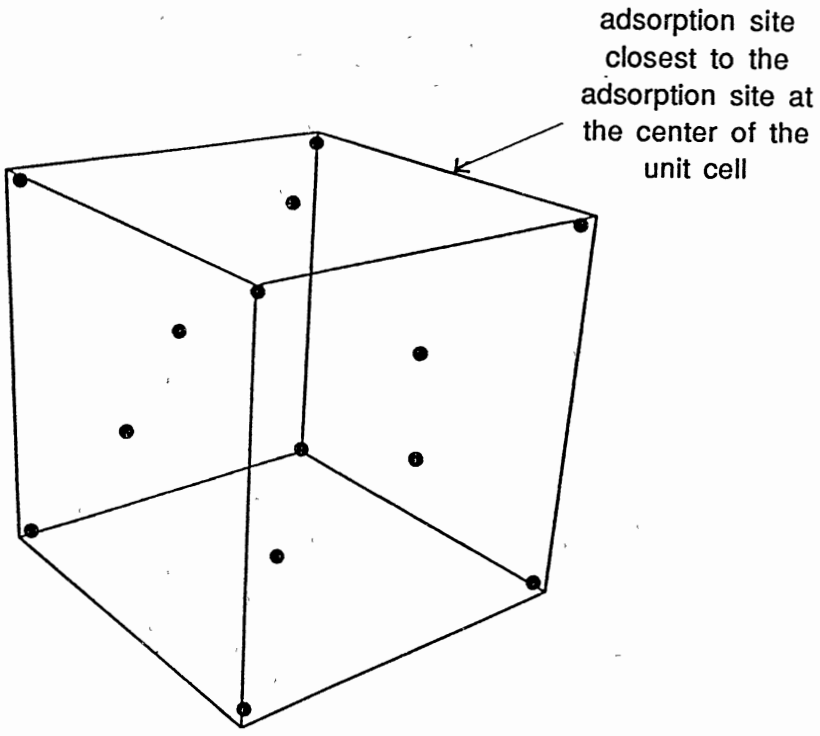


Figure 4. Diagram of a Unit Cell of a Face-Centered Cubic Matrix

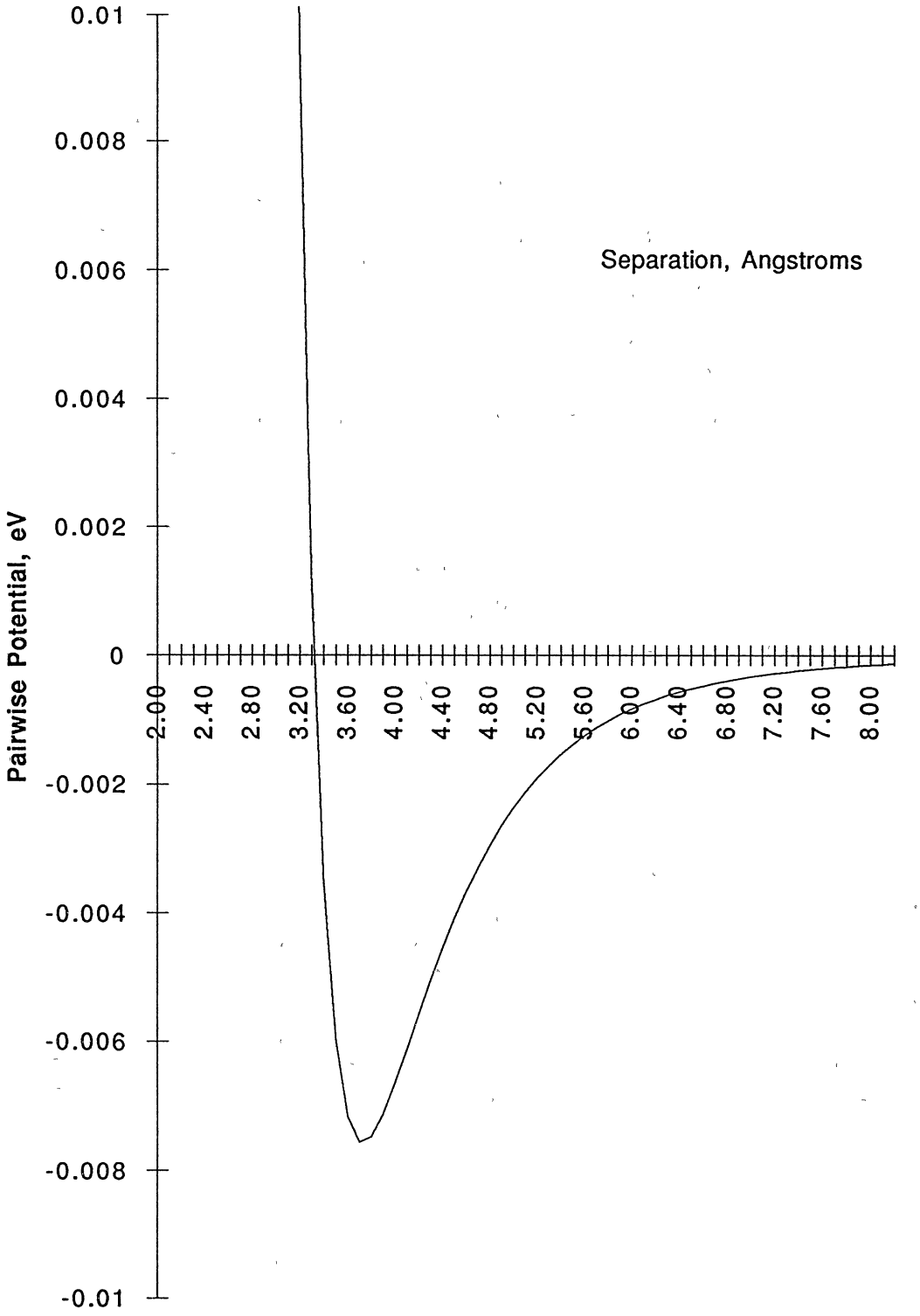


Figure 5. Potential Erergy vs. Diatomic Separation for Xenon-Oxygen

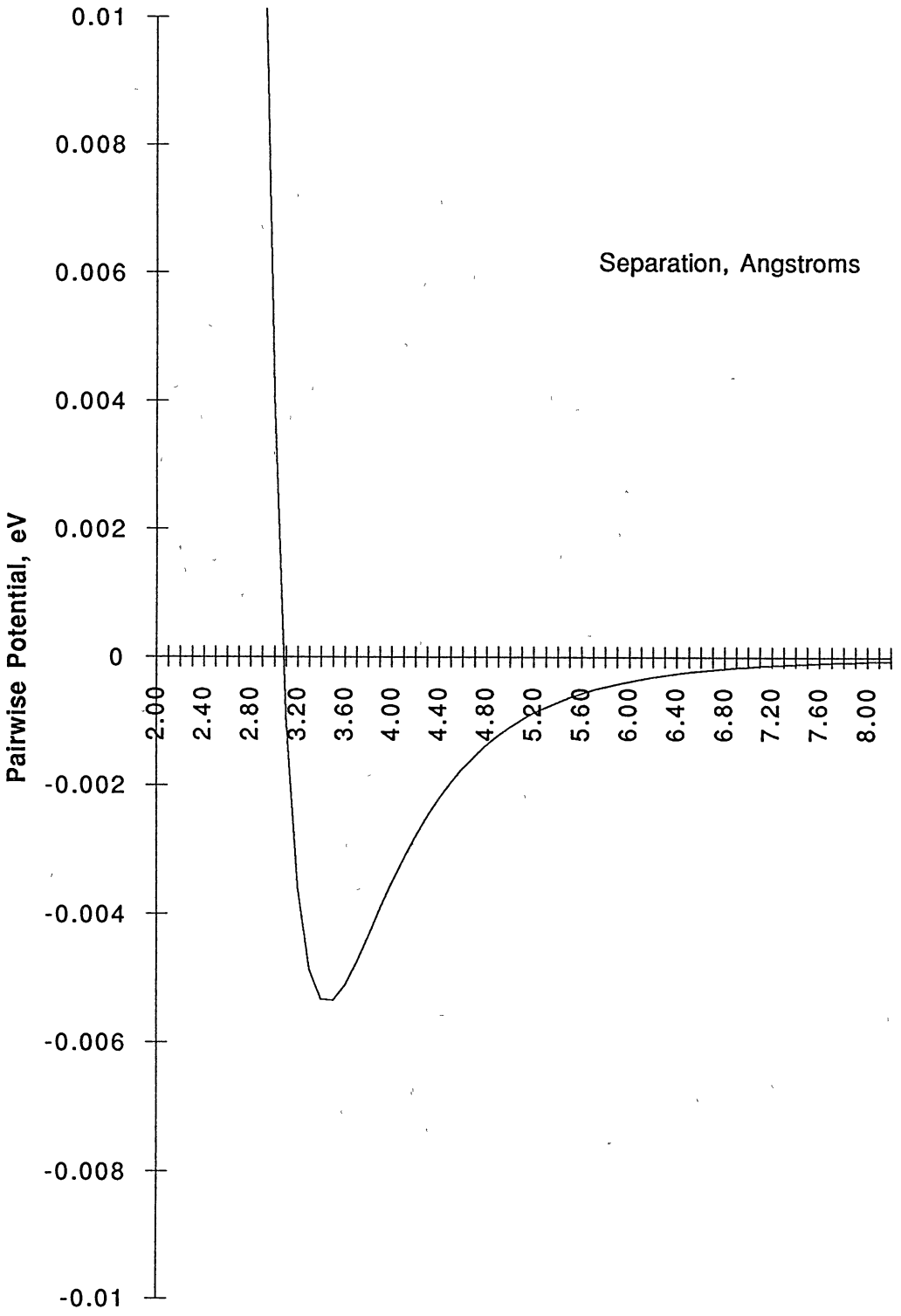


Figure 6. Potential Energy vs. Diatomic Separation for Argon-Oxygen

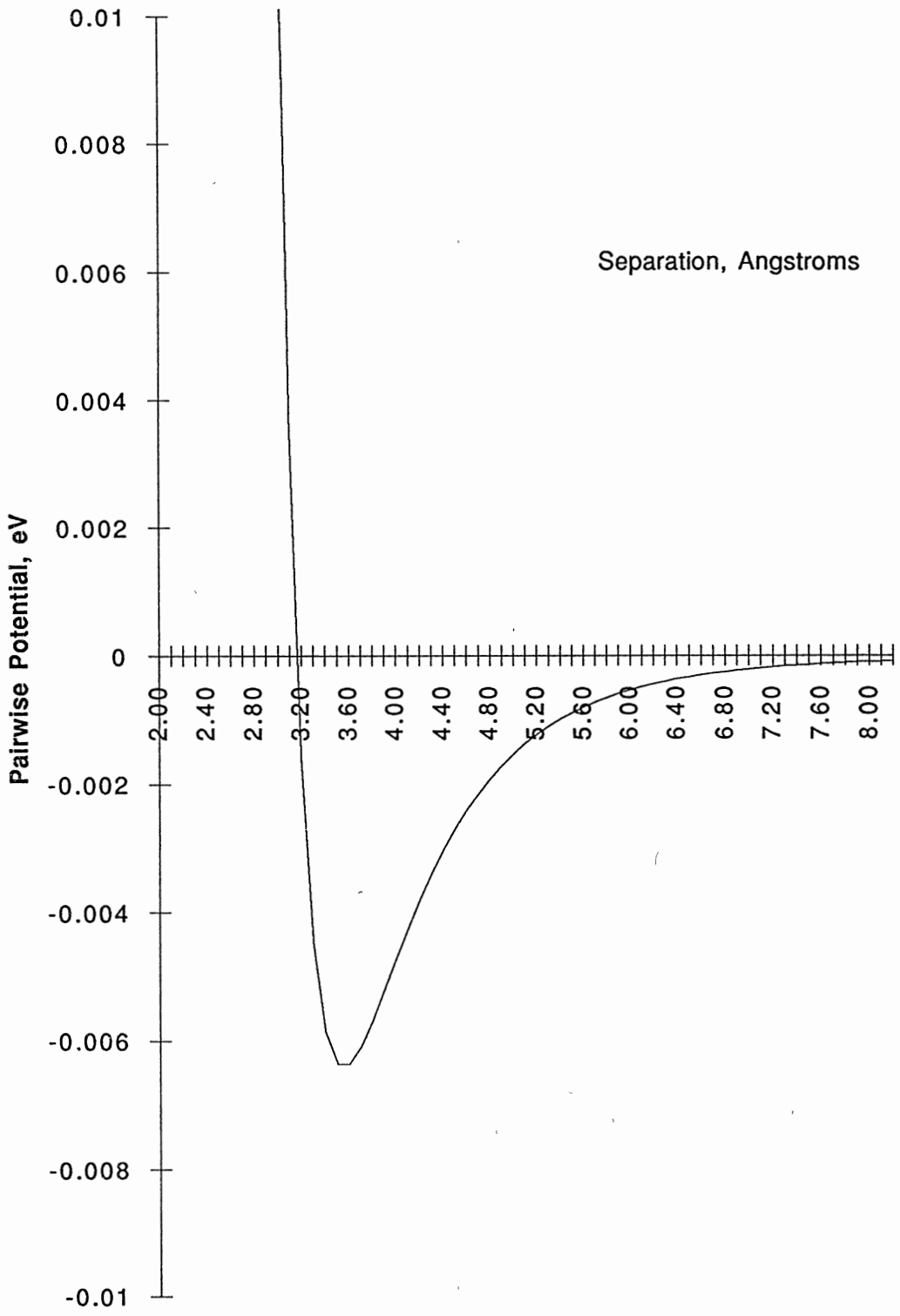


Figure 7. Potential Energy vs. Diatomic Separation for Krypton-Oxygen

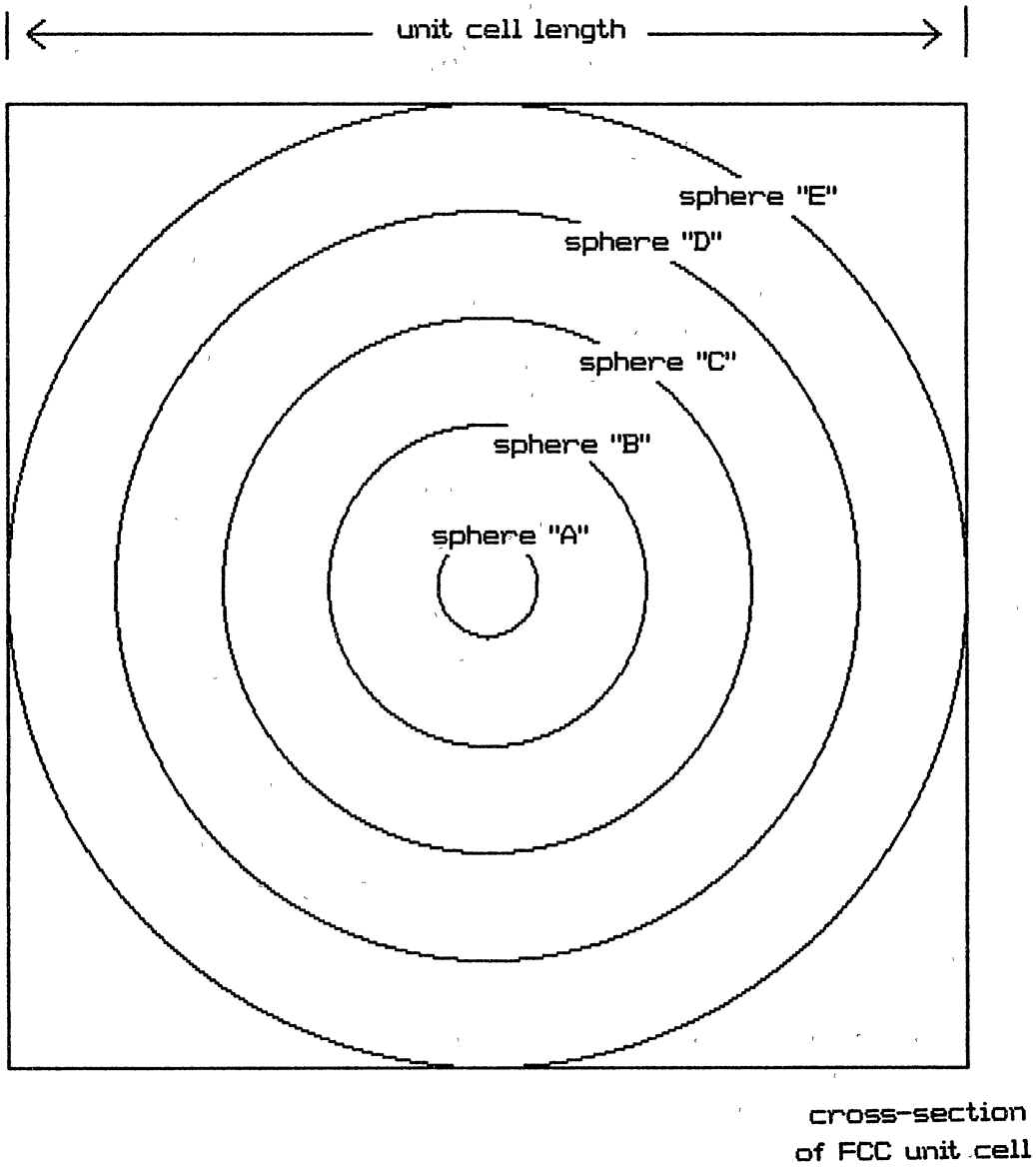


Figure 8. Illustration of Theoretical Dividing Surfaces "A", "B", "C", "D", and "E" Used in Evaluating the Unit Cell for Maximum Barrier to Diffusion From One Adsorption Site to an Adjacent Adsorption Site

Xenon at 100 K

| # MOVES ATTEMPTED | # MOVES ACCEPTED | Minimum Potentials Observed in Dividing Volumes | | | | |
|---|---|---|---|---|---|---|
| | | A | B | C | D | E |
| 1000 | 397 | 0.2934 | 2.7701 | 2.1519 | 2.947 | 3.2327 |
| 5000 | 2087 | 0.2934 | 1.2457 | 2.0837 | 1.7036 | 2.0894 |
| 30000 | 12261 | 0.2934 | 0.9915 | 1.6008 | 1.0405 | 0.9117 |
| 50000 | 20206 | 0.2934 | 0.9915 | 1.6008 | 0.7261 | 0.9117 |
| 100000 | 40004 | 0.2934 | 0.6871 | 1.0983 | 0.7261 | 0.8234 |
| 300000 | 119189 | 0.2264 | 0.5015 | 0.6577 | 0.7261 | 0.6262 |
| 500000 | 198116 | 0.2264 | 0.4879 | 0.6577 | 0.7261 | 0.6262 |
| 1000000 | 396058 | 0.2264 | 0.4164 | 0.6577 | 0.7261 | 0.5581 |
| 1300000 | 514577 | 0.2264 | 0.4164 | 0.6577 | 0.7261 | 0.5581 |

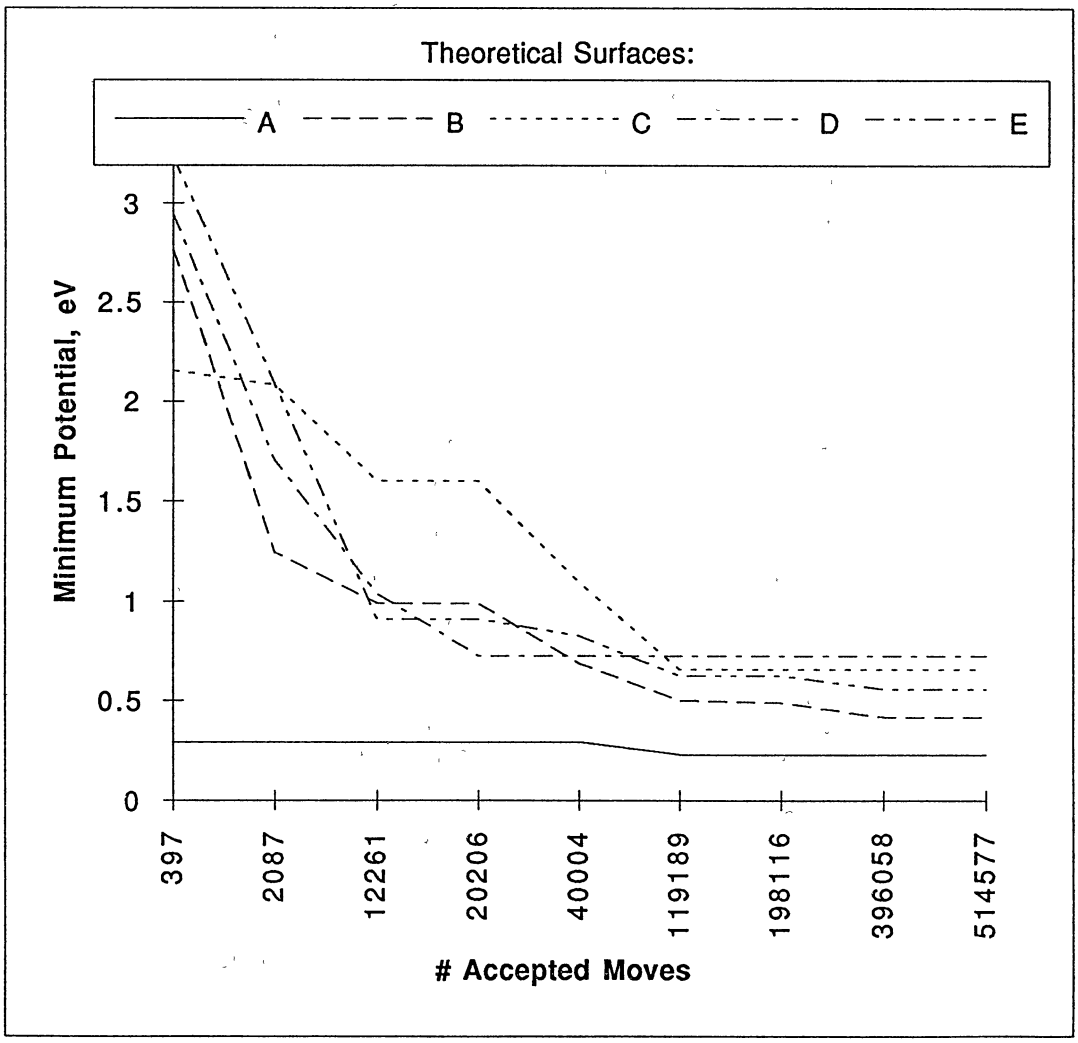


Figure 9. Minimum Potential Energies Observed on Each Dividing Surface in the Xenon Matrix vs. Number of Accepted Moves

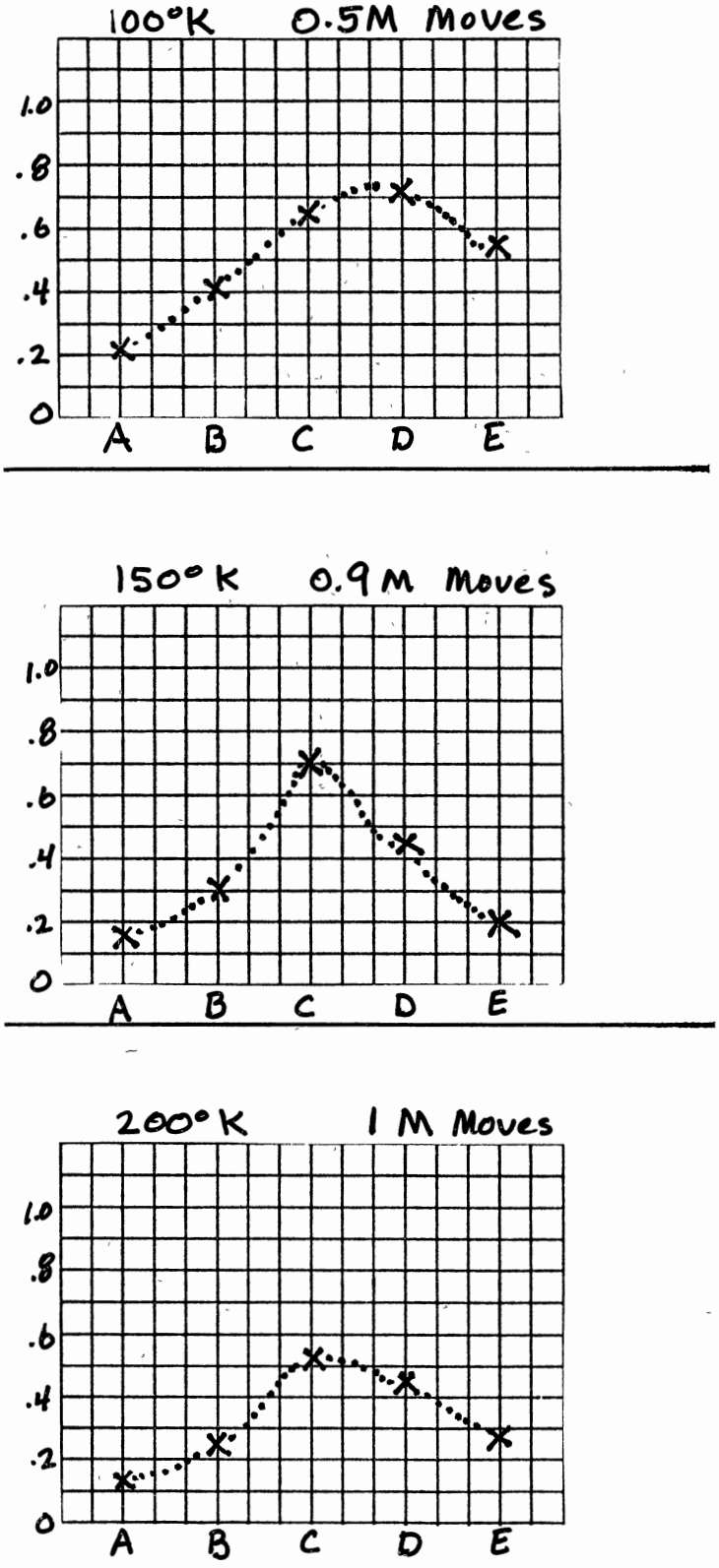


Figure 10. Comparison of Minimum Potential Energies Observed for the Five Dividing Surfaces for Xenon at 100, 150, and 200 K

TEMP = 150 K, FACTORS = 20,45,55,60,45

| #MOVES | #ACCEPTED | %ACCPTD | POTENTIAL MINIMA A | B | C | D | E | NUMS A | B | C | DENOMS A | B | C | D |
|---|---|---|---|---|---|---|---|---|---|---|---|---|---|---|
| 100 | 56 | 56.00% | 0.259 | 1.3[illegible] | [illegible] | | | 2.646 | | | 25.50 | 25.50 | 25.50 | 25.50 |
| 50000 | 14527 | 48.42% | 0.259 | 0.7[illegible] | [illegible] | 0.748 | 0.692 | 0.711 | 2.660 | | 0.057 | 25.58 | 25.58 | 25.58 | 25.58 |
| 70000 | 33195 | 47.42% | 0.259 | 0.7[illegible] | [illegible] | 0.748 | 0.692 | 0.604 | 2.675 | 0 | 0.057 | 25.58 | 25.58 | 25.58 | 25.58 |
| 100000 | 47087 | 47.09% | 0.259 | 0.5[illegible] | [illegible] | 0.748 | 0.692 | 0.604 | 2.670 | 0.001 | 0.057 | 25.58 | 25.58 | 25.58 | 25.58 |
| 300000 | 139693 | 46.56% | 0.170 | 0.3[illegible] | [illegible] | 0.748 | 0.692 | 0.604 | 3492 | 278856 | 0.126 | 49.09 | 49.09 | 49.09 | 49.09 |
| 500000 | 232564 | 46.51% | 0.170 | 0.3[illegible] | [illegible] | 0.748 | 0.692 | 0.604 | 3492 | 278856 | 0.126 | 49.09 | 49.09 | 49.09 | 49.09 |
| 700000 | 324514 | 46.36% | 0.170 | 0.3[illegible] | [illegible] | 0.748 | 0.692 | 0.604 | 3492 | 278856 | 0.121 | 49.10 | 49.10 | 49.10 | 49.10 |
| 1000000 | 463831 | 46.38% | 0.170 | 0.3[illegible] | [illegible] | 0.703 | 0.692 | 0.604 | 4243 | 338856 | 2.271 | 65.96 | 65.96 | 65.96 | 65.96 |
| 1300000 | 602842 | 46.37% | 0.170 | 0.3[illegible] | [illegible] | 0.703 | 0.600 | 0.432 | 4257 | 338856 | 2.275 | 69.81 | 69.82 | 69.82 | 69.82 |
| 1500000 | 696061 | 46.40% | 0.170 | 0.3[illegible] | [illegible] | 0.703 | 0.463 | 0.432 | 4860 | 338869 | 2.275 | 73.87 | 73.87 | 73.87 | 73.87 |
| 1700000 | 788454 | 46.38% | 0.170 | 0.3[illegible] | [illegible] | 0.703 | 0.463 | 0.432 | 4862 | 338894 | 2.275 | 73.884 | 73.884 | 73.884 | 73.884 |
| 2000000 | 926671 | 46.33% | 0.170 | 0.3[illegible] | [illegible] | 0.703 | 0.463 | 0.199 | 4865 | 338916 | 2.275 | [illegible] | [illegible] | [illegible] | [illegible] |

TEMP = 150 K, FACTORS = 40,50,60,70,70

| #MOVES | #ACCEPTED | %ACCPTD | POTENTIAL MINIMA A | B | C | D | E | NUMS A | B | C | DENOMS A | B | C | D |
|---|---|---|---|---|---|---|---|---|---|---|---|---|---|---|
| 100 | 96 | 96.00% | 0.387 | | | | | 1490[illegible] | | | 1.593 | 1.593 | 1.593 | 1.593 |
| 1000 | 780 | 78.00% | 0.358 | 1.219 | 1[illegible] | | | 6[illegible]045 | | | 1.813 | 1.813 | 1.813 | 1.813 |
| 5000 | 3589 | 71.78% | 0.358 | 1.219 | 2.917 | 1040. | | 6[illegible]045 | | | 1.813 | 1.813 | 1.813 | 1.813 |
| 30000 | 19188 | 63.96% | 0.358 | 0.880 | 1.051 | 0.742 | 1.592 | 6[illegible]045 | | | 1.813 | 1.813 | 1.813 | 1.813 |
| 50000 | 31159 | 62.31% | 0.358 | 0.880 | 1.051 | 0.742 | 1.592 | 6[illegible]045 | | | 1.813 | 1.813 | 1.813 | 1.813 |
| 70000 | 43188 | 61.70% | 0.358 | 0.880 | 1.051 | 0.742 | 1.592 | 6[illegible]045 | | | 1.813 | 1.813 | 1.813 | 1.813 |
| 100000 | 61079 | 61.08% | 0.358 | 0.880 | 1.051 | 0.742 | 1.592 | 6[illegible]045 | | | 1.813 | 1.813 | 1.813 | 1.813 |
| 300000 | 179707 | 59.90% | 0.358 | 0.463 | 0.538 | 0.742 | 0.676 | 6[illegible]045 | 3E+06 | 2E+00 | 1.813 | 1.823 | 1.823 | 1.823 |
| 500000 | 298285 | 59.66% | 0.358 | 0.463 | 0.538 | 0.742 | 0.650 | 6[illegible]045 | 3E+06 | 2E+00 | 1.813 | 1.823 | 1.823 | 1.823 |
| 700000 | 416752 | 59.54% | 0.358 | 0.463 | 0.538 | 0.742 | 0.650 | 6[illegible]045 | 3E+06 | 2E+00 | 1.813 | 1.823 | 1.823 | 1.823 |
| 1000000 | 594775 | 59.48% | 0.358 | 0.463 | 0.538 | 0.742 | 0.650 | 6[illegible]045 | 3E+06 | 2E+00 | [illegible] | [illegible] | [illegible] | [illegible] |

Figure 11. Raw Data Collected for Xenon and Argon at 150 K Showing Changes in Minimum Potential and Flux Numerators and Denominators vs. Number of Accepted Moves

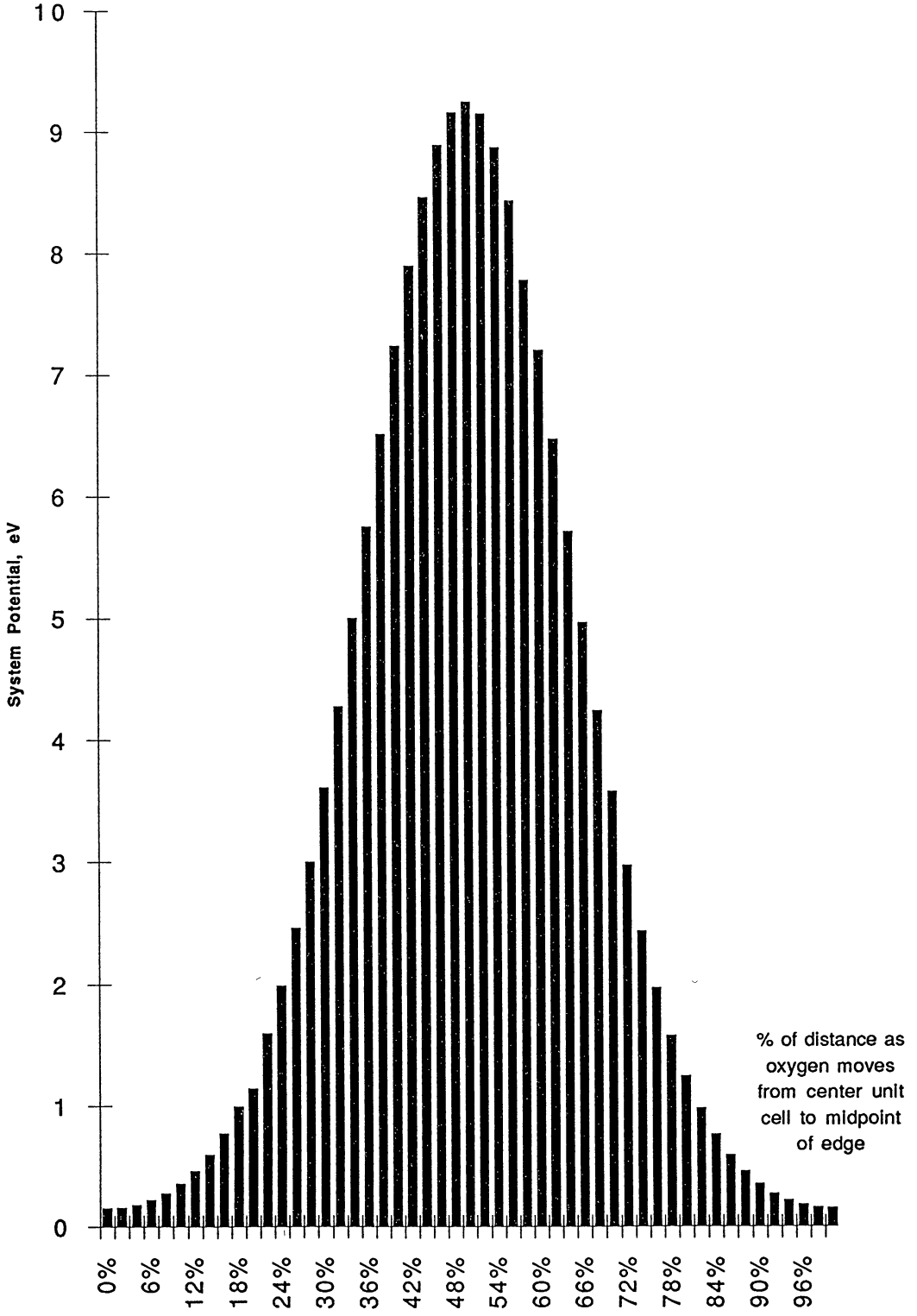


Figure 12. Potential Energy vs. Oxygen Movement Between Two Adjacent Adsorption Sites in a Fixed Xenon Matrix

Xenon

| Temp, K | D(min), cm2/s, "C" | 1/T | ln(D) |
|---|---|---|---|
| 100 | 6.58E-29 | 0.01000 | -64.890933 |
| 150 | 2.98E-22 | 0.00667 | -49.5649487 |
| 200 | 1.38E-13 | 0.00500 | -29.6115227 |

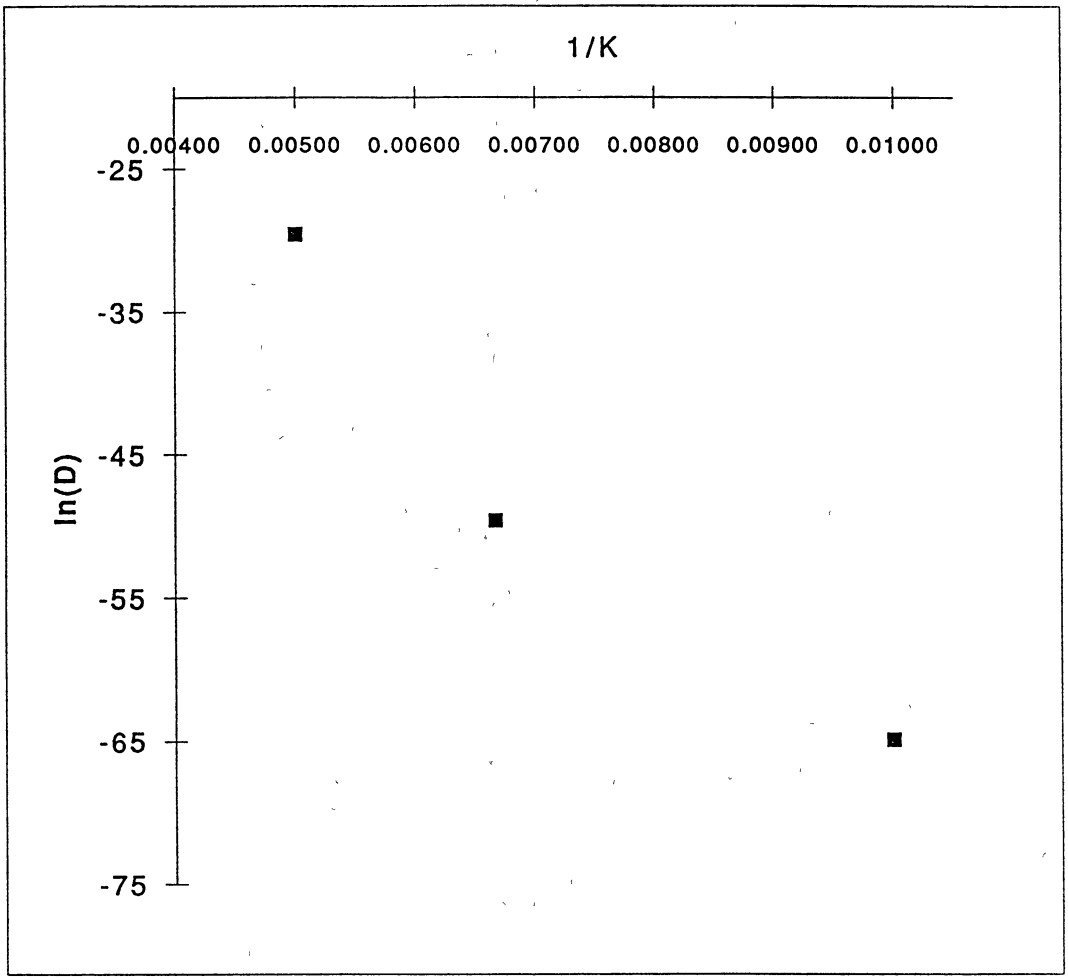


Figure 13. Plot of Natural Log Diffusion Rate (Theoretical) vs. 1/T (K) for Xenon

VITA

M. Beth Ford

Candidate for the Degree of

Master of Science

Thesis: THEORETICAL STUDIES OF OXYGEN DIFFUSION IN FACE-CENTERED CUBIC MATRICES OF XENON, ARGON, AND KRYPTON

Major Field: Analytical Chemistry

Biographical:

Personal Data: Born in Hobart, Oklahoma, November 23, 1959, the daughter of William L. and Sylvia L. Bolding.

Education: Graduated from Hobart Senior High School, Hobart, Oklahoma, in May, 1978; received Bachelor of Science Degree in Chemistry from Oklahoma State University in May, 1982; completed requirements for the Master of Science degree at Oklahoma State University in December, 1992.

Professional Experience: Summer Student, Conoco, Inc., June, 1980, to August, 1980, and June, 1981, to August, 1981; Teaching Assistant, Department of Chemistry, Oklahoma State University, August, 1981 to December, 1981; Chemist, Conoco, Inc., June, 1982, to present.